I&EC research
Industrial & Engineering Chemistry Research
pubs.acs.org/IECR
Article

MTO with SAPO-34 in a Fixed-Bed Reactor: Deactivation Profiles

Diego Zapater, Javier Lasobras, Jaime Soler, Javier Herguido, and Miguel Menéndez*

Cite This: *Ind. Eng. Chem. Res.* 2021, 60, 16162−16170
Read Online
ACCESS | Metrics & More | Article Recommendations

ABSTRACT: Methanol-to-olefins is a promising process that has attracted the attention of many research groups in the last years. Zeolites are the primary catalyst for this process, and SAPO-34 is one of the most used because of its high selectivity toward C_2−C_4 olefins. As a drawback, it deactivates quickly and forces the process to work alternately using reaction and regeneration cycles. The mechanism by which SAPO-34 deactivates is still on debate, and further research needs to be done. In this study, the evolution of the deactivation profile for an SAPO-34-based catalyst was studied in a fixed-bed reactor. To achieve that, the catalyst bed was extracted after each experiment and divided in sections of 2 cm. For each section, CO_2 adsorption, thermogravimetric analysis, and ammonia temperature-programmed desorption were performed.

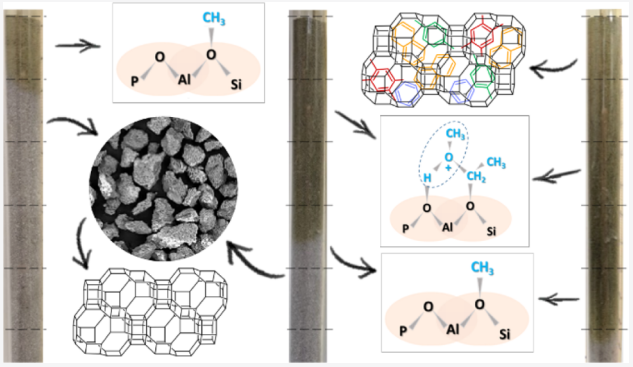

INTRODUCTION

Light olefins (ethylene and propylene) are key components in chemical industry as they are commodities used for a wide range of applications. Some examples of ethylene uses are polyethylene, vinyl chloride, ethylene oxide, glycol, and other derivative chemicals such as detergents, thickeners, solvents, and plastics. In the case of propylene, it is used to produce polypropylene, acrylonitrile, acrylic acid, and other derivative chemicals.

Traditionally, olefins are mainly produced by the cracking of crude oil, naphtha, or natural gas. Due to the limitation of these reserves and the tendency to move toward a more sustainable future, new routes and processes have been proposed. One of them, if not the best, is the methanol-to-olefins process (MTO), in which methanol obtained from coal or natural gas is used as the raw material to produce mainly ethylene and propylene.

Many institutions and companies have put their focus into the MTO reaction since it was first proposed by Mobil Corporation in 1977,[1] and a lot of progress has been achieved regarding the reaction mechanism, catalyst synthesis, and process research. In particular, the first MTO reactions took place with the ZSM-5 catalyst,[2,3] but Union Carbide researchers showed the excellent performance and selectivity to C_2−C_4 olefins of the SAPO-34 catalyst. This behavior is produced by the smaller pore size of SAPO-34 (3.5 Å[4]) than that of ZSM-5 (5.6 Å[5]), which increases the diffusional limitations of bigger hydrocarbons in the first one.

The reaction network through which olefins are obtained is still on debate. However, some mechanisms are commonly accepted. In the 1980s, the alkene-based pathway was proposed by Dessau,[6,7] but due to the recognition of the aromatic presence, the hydrocarbon pool mechanism was proposed by Dahl and Kolboe in the 1990s.[8] Lately, the role of methylbenzenes and other carbenium ions as intermediates was discovered,[9−11] and some modifications to it were carried out by Svelle and co-workers[12−14] when they proposed the dual-cycle mechanism. This mechanism, modified through the later years, has been accepted as the most probable route of olefin formation till now.

The main disadvantage of SAPO-34 zeolite is its fast deactivation, caused by the gradual transformation of active intermediate species to less active polycyclic aromatics and finally coke. Furthermore, the deactivating species could also cause pore blockage, making the deactivation process more complex.[10,15] Wragg et al. assumed that all aromatic and coke species in the SAPO-34 catalyst cover Brønsted acid sites. Therefore, the deactivation process is caused by the transformation of active species to coke species, which reduces the available active acid sites.[16]

Due to the importance of deactivation, the aim of this work is to study the evolution of the deactivation profile of the catalyst bed in a fixed-bed reactor through time-on-stream (TOS), which was carried out by analyzing the micropore

Received: July 9, 2021
Revised: October 15, 2021
Accepted: October 17, 2021
Published: October 27, 2021

https://doi.org/10.1021/acs.iecr.1c02718
Ind. Eng. Chem. Res. 2021, 60, 16162−16170

volume, acidity, and total amount of species formed for each section of the bed.

MATERIALS AND METHODS

Catalyst Preparation. An agglomeration is required in order to reduce the pressure drop in the fixed bed caused by the 2 μm particle size of the zeolite. Agglomeration tests were carried out to find which combination of zeolite, clay, and oxide provides the largest fraction of the biggest particle size.

Several catalysts were prepared for the agglomeration of HSAPO-34 (ACS Material, 2 μm), a clay: bentonite (Sigma-Aldrich, dp < 100 μm), attapulgite (MYTA, dp < 100 μm), sepiolite (MYTA, dp < 100 μm), montmorillonite (Alfa Aesar, dp < 100 μm), or boehmite (Sasol, dp < 100 μm) and an oxide: silica (SIPERNAT, 106 < dp < 250 μm) or alumina (Puralox, 45 < dp < 250 μm). The weight ratio in the preparation is maintained at 50/30/20 (zeolite/clay/oxide) for all of them.

The agglomeration was carried out by wet impregnation,[17] followed by sieving to obtain the particle size distribution. The selected particle size of the final catalyst was the 160−315 μm fraction to maintain the pressure drop below 0.2 bar in the catalytic tests.

Catalyst Characterization. The fresh catalyst particle size distribution was studied by sieving, its composition by X-ray fluorescence spectroscopy (XRF, THERMO ELECTRON, ARL mod. ADVANT'XP), and its superficial composition and morphology by field-emission scanning electron microscopy (FESEM, MERLIN, Carl Zeiss).

The evolution of the catalyst bed along TOS was studied by visual methods (macroscopic changes in the catalyst): CO_2 adsorption (Autosorb iQ3, Quantachrome) for the evolution of the specific surface and microporous structure; thermogravimetric analysis (TGA, Libra F1, NETZSCH) with a first step of a N_2 atmosphere between 25 and 750 °C and a second step of an air atmosphere at 750 °C for the characterization of the species contained within the catalyst; and temperature-programmed desorption (TPD) of ammonia, following the m/z = 16 signal with a mass spectrometer (ThermoOnix ProLab), for acidity measurements.[17]

It is noteworthy that due to the size of some of the zeolite pores (3.7−7.4 Å[4]), CO_2 instead of N_2 has been selected for the specific surface analysis due to its kinetic diameter being smaller (3.3 vs 3.64 Å, respectively[18,19]). For the same reason, in the acidity measurement, NH_3 and not pyridine (2.6 vs 5.7 Å, respectively[20,21]) has been selected because the latter could not enter the pores of the zeolite.

Experimental Setup. Liquid methanol was fed through a peristaltic pump (D-25Vplus, DINKO) to an evaporator, where it was mixed with nitrogen as the carrier gas to maintain a methanol partial pressure of 0.66 bar. A secondary line of nitrogen as the diluent is set before the reactor to modify the total amount of gas fed to it or to feed only nitrogen, if necessary. The mixture was fed to a cylindrical quartz reactor (30 cm high and 1 cm of internal diameter) with a quartz plate as the gas distributor and support of the catalyst bed. The catalyst load was 6.0 g, and W/F_{MeOH} was maintained at 11.35 g·h·mol^{-1}. Heat transfer to the reactor was provided by an electric oven around the reactor. The reaction temperature was set to be 500 °C, controlled by a PID controller, and measured by a thermocouple located at the center of the catalyst bed. The pressure in the reactor was set to be atmospheric (1 bar) and measured by a pressure sensor (VAP 445, Digitron). Downstream of the reactor, a pair of condensers were set in a cool bath at −15 °C to recover both the water produced in the reaction and the unreacted methanol. Catalyst characterization was carried out offline by the techniques specified previously.

Due to the fast deactivation of the catalyst,[9,22−26] the methanol−nitrogen mixture was fed as pulses. The experimental procedure was as follows: (i) the reactor is heated to 500 °C after a slope of 5 °C, while 300 cm^3 (STP)·min^{-1} nitrogen is fed through the secondary line to the catalyst bed; (ii) when the reaction temperature is reached, the secondary nitrogen flow is stopped, and 300 cm^3 (STP)·min^{-1} of the methanol−nitrogen mixture is fed for 100, 200, 300, 600, 900, and 3600 s of TOS; (iii) after that time, the feed of the methanol−nitrogen mixture is stopped, and 300 cm^3 (STP)·min^{-1} nitrogen is fed through the secondary line again, while the reactor cools down; (iv) when the catalyst bed is at room temperature, the reactor is extracted, and some images of the appearance of the catalyst bed are taken; and after that, (v) the catalyst is extracted by 2 cm height sections, each corresponding to one sample.

RESULTS AND DISCUSSION

The most relevant results are presented in this section. These include the agglomeration tests and the characterization of the catalyst bed for each time and position.

Agglomeration Tests. The agglomeration by wet impregnation was effective with bentonite as the clay and alumina or silica as the oxide. The agglomeration produces a catalyst with a bigger particle size than that of the commercial zeolite, with an optimum composition of 50 (HSAPO-34)/30 (bentonite)/20 (alumina). For this composition, 75 wt % obtained catalyst has a particle size distribution between 160 and 315 μm.

Catalyst Characterization at TOS = 0 s. The freshly agglomerated catalyst was characterized by CO_2 adsorption, FESEM, XRF, and TPD of NH_3.

The CO_2 adsorption allows the characterization of the microporous structure of the catalyst, which is a key parameter in MTO because the production of olefins from methanol is a result of the shape selectivity of the zeolite.[27−29] The results obtained by the density functional theory method are shown in Table 1.

Table 1. Surface Area and Micropore Volume of the Samples Obtained by CO_2 Adsorption

sample	HSAPO-34	bentonite	alumina	fresh catalyst	theoretical 50/30/20
S_{CO2} ($m^2 \cdot g^{-1}$)	1271.8	93.2	192.5	705.0	702.4
$V\mu p$ ($cm^3 \cdot g^{-1}$)	0.38	0.04	0.05	0.21	0.21

The agglomerated catalyst has a specific surface area of 705.0 $m^2 \cdot g^{-1}$ and a micropore volume of 0.21 $cm^3 \cdot g^{-1}$, similar to the values obtained theoretically as a weighted mean of its three components. This was a result of the preparation process, in which the three solids agglomerate physically and the micropore structure of the zeolite was not affected. Additionally, the CO_2 adsorption analysis showed that pore distribution of the catalyst is mainly formed by 3.4, 5.2, and 7.4 Å pores, the same as for HSAPO-34 zeolite.

https://doi.org/10.1021/acs.iecr.1c02718
Ind. Eng. Chem. Res. 2021, 60, 16162−16170

The morphology and surface composition of the samples were analyzed by FESEM and are shown in Figure 1 and Table 2, respectively.

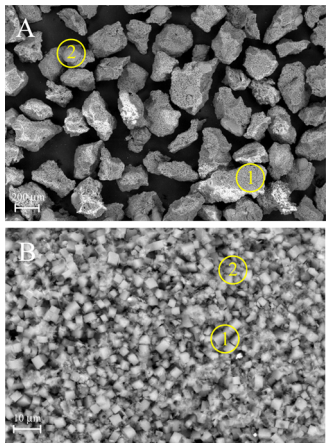

Figure 1. SEM Images of the agglomerated catalyst. Scale: 200 (A) and 10 μm (B).

The agglomeration was effective, as can be seen in Figure 1. The particles of the catalyst (Figure 1A-1) have an irregular morphology but bigger size than its three components. These particles are formed mainly by agglomerated HSAPO-34 (cubic-shaped particles, Figure 1B-1) and bentonite (sheet-shaped particles, Figure 1B-2), and alumina (spherical-shaped particles, Figure 1A-2) is attached to some particles. In the following table (Table 2), the results of surface analysis for the previous four zones of SEM images are presented.

The surface elemental composition analysis reveals that all solids are mainly formed by oxides: HSAPO-34 particles contain Al, P, and Si; bentonite has Si, Al, and Fe; and alumina is completely Al.

The elemental composition of the fresh catalyst was analyzed by XRF, and the results obtained are shown in Table 3.

As for XRF, the elemental composition analysis reveals that the catalyst is mainly formed by oxides of Al, Si, and P. If XRF results are compared to FESEM results, the major discrepancies are found in Al (23.2 vs 25.1), Si (12.5 vs 10.0), and Fe (1.0 vs 2.6), the main components of bentonite. This could be attributed to the bentonite heterogeneous nature, as FESEM average results are calculated with the data of only one zone of each component.

The capacity for transforming methanol into olefins is strongly related to the acid strength of the zeolite,[30−34] which can be measured by the TPD of ammonia.[35−37] The representation of the acidity for the fresh catalyst and its components is shown in Figure 2.

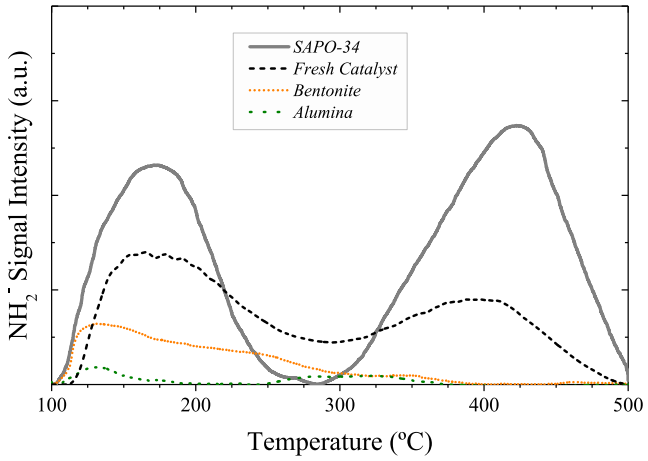

Figure 2. Acid site distribution for the fresh catalyst and its components.

Table 3. Elemental Composition of the Fresh Catalyst by XRF (wt %)

O	Na	Mg	Al	Si	P	Fe	others
51.0	0.4	0.5	23.2	12.5	11.1	1.0	0.3

The acidity of the catalyst comes from the contribution of its components. HSAPO-34 exhibits highly weak and strong acidity with peaks around 175 and 425 °C, respectively. Bentonite and alumina show lower acidity than HSAPO-34, and only weak acid sites between 125 and 300 °C for the first one and 130 °C for the second one. The acidity of the fresh catalyst is a contribution of weak acid sites (between 150 and 250 °C) and strong acid sites (between 325 and 450 °C), but some medium acidity is observed at 300 °C.

The strength of these acid sites can be quantified to obtain the acid site concentration of each type (Table 4).

As can be observed, the acid site concentration for the fresh catalyst differs between the amount measured and the theoretical value calculated, the former being greater for the weak acid sites and the latter being bigger for the strong acid sites. This could be a result of some ion exchange phenomena between the zeolite and the bentonite, as some authors suggested.[38−41] However, if the total acid site concentration is taken into account, the measured and theoretical values are close (8.92 and 8.61, respectively).

Catalyst Deactivation Profile with TOS. As methanol is fed and MTO reactions take place, the catalyst undergoes an evolution with the TOS. This evolution is a result of the changes in the structure, acidity, and composition of the catalyst and can be noted even in a macroscopic scale. The macroscopic evolution of the catalyst bed with the TOS is shown in Figure 3.

Table 2. Surface Elemental Composition of the Samples by FESEM

location in Figure 1	sample	O	Na	Mg	Al	Si	P	Fe
A-1	HSAPO-34 + bentonite	52.1	0.5	0	20.8	6.7	19.1	0.7
A-2	Al_2O_3	44.0	0	0	54.0	2.1	0	0
B-1	HSAPO-34	54.0	0.5	0	19.1	8.2	16.9	1.0
B-2	Bentonite	48.3	0.6	0.9	15.9	18.2	9.0	6.9
theoretical 50/30/20		50.3	0.5	0.3	25.1	10.0	11.1	2.6

https://doi.org/10.1021/acs.iecr.1c02718
Ind. Eng. Chem. Res. 2021, 60, 16162−16170

Table 4. Acid Site Concentration by Ammonia Desorption

acid sites (mmol $NH_3 \cdot g^{-1}$)	HSAPO-34	bentonite	alumina	fresh catalyst	theoretical 50/30/20
weak (<300 °C)	6.53	2.61	0.31	5.31	4.12
strong (>300 °C)	8.97	0.08	0.07	3.61	4.49

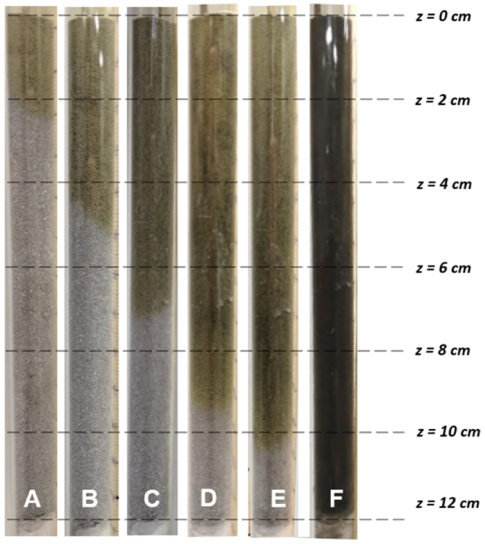

Figure 3. Macroscopic evolution of the catalyst bed after (A) 100 s, (B) 200 s, (C) 300 s, (D) 600 s, (E) 900 s, and (F) 3600 s of TOS.

As can be seen, as methanol is fed and reactions take place, the initial light gray appearance of the catalyst is replaced by a dark green tone. This change could be attributed to a structural alteration due to the formation, evolution, and deposition of species with different natures and reactivities. Initially, these species are more active, but as the reaction goes on and the deactivation profile descends, they evolve to others less active and with a higher molecular weight.[32] This mechanism agrees with the "cigar burn" model, most easily visualized as a plug-flow reactor.[42]

From the deactivation profile, additional information regarding the macroscopic evolution can be extracted. Figure 4A shows the vertical position and mass of the catalyst that has suffered a visual change with the TOS. Additionally, Figure 4B represents their derivative with respect to time.

From Figure 4B, it can be seen that the deactivation rate was not constant. It was around 1.4 $cm \cdot min^{-1}$ (0.69 $g_{cat} \cdot s^{-1}$) until 300 s, but it dropped down rapidly to 0.45 $cm \cdot min^{-1}$ (0.24 $g_{cat} \cdot s^{-1}$) at 600 s and 0.24 $cm \cdot min^{-1}$ (0.12 $g_{cat} \cdot s^{-1}$) at 900 s. Finally, at 3600 s, it reached 1×10^{-3} $cm \cdot min^{-1}$ (1×10^{-5} $g_{cat} \cdot s^{-1}$), which could be considered zero. This evolution of the deactivation rate could be attributed to a secondary mechanism observed at 500 °C in previous studies and by other authors.[17,43] By this mechanism, when methanol was fed to a deactivated catalyst (with a high TOS), it reacted to produce methane and carbon monoxide. This means that even when the catalyst is deactivated for MTO, it is still active for this secondary process. The mechanism involved in the secondary reactions is not fully understood, but it is believed to be caused by the remaining acidity of the catalyst or the presence of iron in the bentonite.

The macroscopic evolution of the catalyst bed can be understood as a change in the micropore structure of the catalyst, which is the key to the shape selectivity for the MTO process. This change can be studied by the evolution of the micropore volume with the TOS (Figure 5). A similar trend has been obtained for the specific surface area, as there was a proportional relation between both of them.

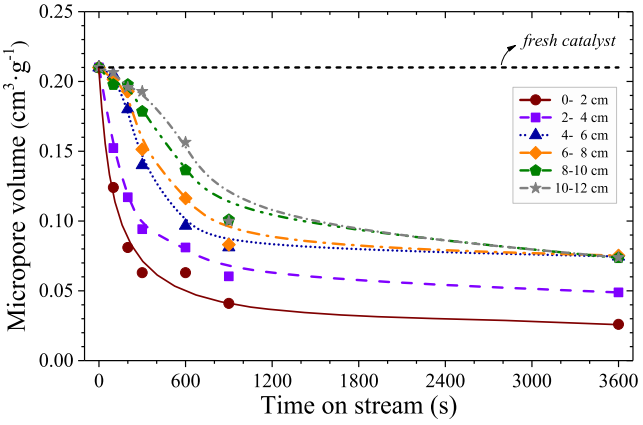

Figure 5. Micropore evolution with the TOS.

Because the reaction takes place first in the upper sections of the catalyst bed, it is expected for these to lose micropore volume before the lower sections. As can be seen in Figure 5, the section between 0 and 2 cm has lost 70% of its initial pore

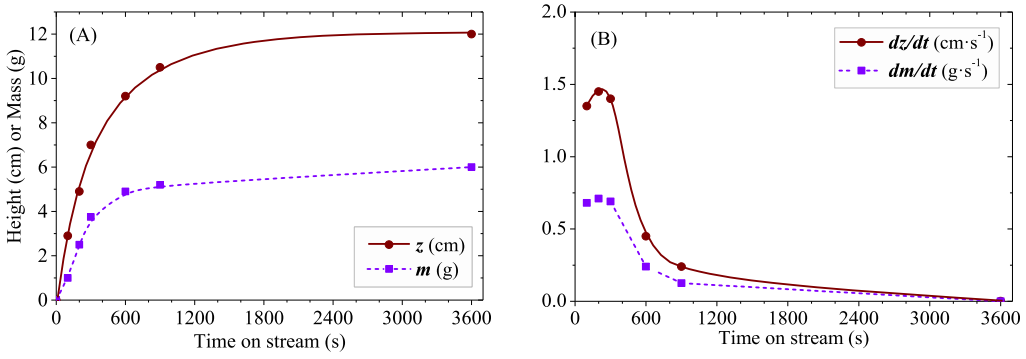

Figure 4. Position (A) and forward velocity (B) of the deactivation profile in the catalyst bed as a function of the TOS (regarding the position and catalyst mass).

https://doi.org/10.1021/acs.iecr.1c02718
Ind. Eng. Chem. Res. 2021, 60, 16162−16170

volume after 300 s, but the section between 4 and 6 cm only has lost 30% and the one between 10 and 12 cm just a 5%. This behavior could be extended to all sections of the catalyst bed for all TOS values.

When the catalyst bed was completely deactivated (3600 s), not all sections of the bed had the same micropore volume. The 0−2 cm section ended up with 0.026 $cm^3 \cdot g^{-1}$, the 2−4 cm section with 0.045 $cm^3 \cdot g^{-1}$, and sections below 4 cm with a volume around 0.072 $cm^3 \cdot g^{-1}$. This could mean that 3600 s of TOS could not be enough to reach a homogeneous deactivation in the whole catalyst bed or that all sections of the catalyst deactivate in a different way.

The evolution of the micropore volume was mainly caused by the appearance of carbonaceous species. Identifying these species is a complex matter since it could be hydrocarbons between C_1 and C_{16}, with single or double bonds and cyclic or linear. Due to this diversity of species, it was decided to classify them according to their volatility, whether they leave the catalyst structure in a N_2 atmosphere from 30 to 750 °C (volatile) or in an air atmosphere at 750 °C (nonvolatile). The evolution of volatile species with TOS is shown in Figure 6.

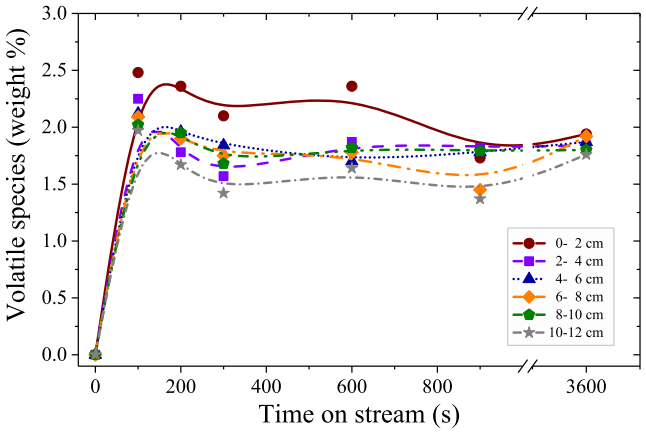

Figure 6. Volatile species evolution with TOS.

The evolution of volatile species presented a clear trend over time. According to this, there is a rapid initial formation of volatile species when the reaction profile reaches each of the bed heights. The rapid initial appearance of these species corresponds to the formation of methoxyl groups in the acid centers of the catalyst as a result of the adsorption reaction of methanol and dimethyl ether,[31] as is shown in Figure 7.

Once these groups have been formed, a series of consecutive reactions take place over them, leading to the propagation of the hydrocarbon chain until a specific size is reached, at which

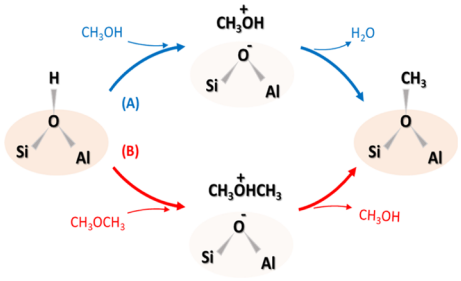

Figure 7. Methoxyl group formation by the reaction of methanol (A) or dimethyl ether (B).

point (if sterically possible) the desorption of the product occurs,[31] as is shown in Figure 8.

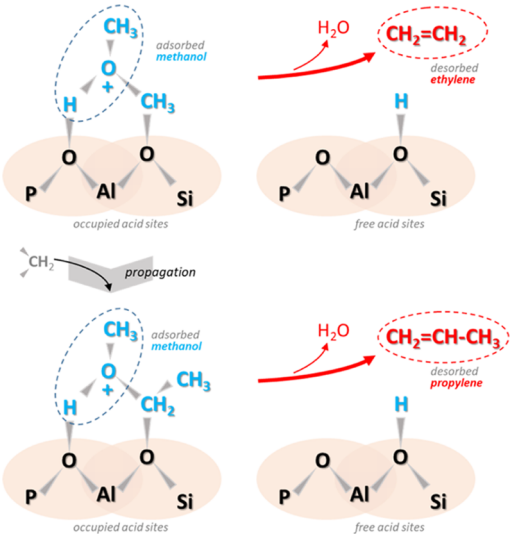

Figure 8. Propagation and desorption of product mechanisms.

It was observed that the concentration of volatile species remained approximately constant, which implies that an equilibrium was reached between their formation and desorption rates. This can be seen in Figure 6 since for all bed heights, the final concentration of volatile species is between 1.5 and 2.5% by weight. Additionally, in those sections to which the reaction profile has not reached, there is also the presence of volatile species, which could be reaction products from the upper zones that have been adsorbed on the acid sites.

The evolution of nonvolatile species with TOS is shown in Figure 9.

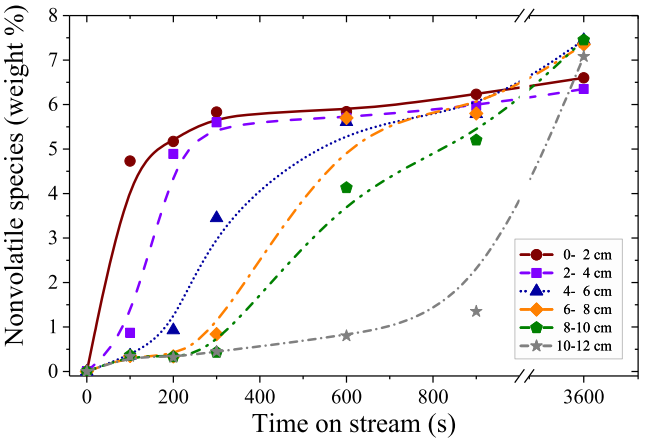

Figure 9. Non-volatile species evolution with TOS.

The evolution of nonvolatile species differs from that observed in volatile species since these nonvolatile species include large hydrocarbons (more than five carbon atoms) and molecular carbon (coke). Due to their size or nature, they are not able to be desorbed, so they are retained in the acidic center where they form. Due to this, their constant accumulation occurs, which means a progressive increase in their concentration over time, as observed in Figure 9. This

https://doi.org/10.1021/acs.iecr.1c02718
Ind. Eng. Chem. Res. 2021, 60, 16162−16170

effect is more pronounced in the first sections of the bed as these are the ones with more TOS.

When the catalyst is deactivated (at 3600 s), the concentrations of nonvolatile species in the catalyst bed are similar for all heights of the bed, which would indicate that there is a maximum concentration of these species admissible by the catalyst, from which it would be totally deactivated. According to the results obtained, this maximum could be between 6.5 and 7.5 wt %.

In this way, from the results obtained by TGA, it is possible to classify the species that cause the catalyst deactivation as volatile and nonvolatile. The former form rapidly when methanol comes in contact with the acid sites of the catalyst and are responsible for the production of lower-molecular-weight hydrocarbons (up to five carbon atoms) such as light olefins. In addition to this, they reach a balance between the rate at which they form and the rate at which they are desorbed from acid sites, which makes their concentration in the solid remain approximately constant (between 1.75 and 2.0%).

The nonvolatile species, which are known to evolve from the previous ones,[44] accumulate in the acid sites where they form as they are not capable of being desorbed. This situation causes pore blockage of the catalyst and its consequent deactivation when their concentration reaches a maximum value (between 6.5 and 7.5 wt %).

The decrease of the micropore structure is caused by the formation of hydrocarbon species inside the pores of the catalyst. These species are composed of adsorbed methanol or dimethyl ether to large hydrocarbons but are formed mainly in the acid sites of the catalyst.

To study how deactivation occurred alongside the catalyst bed, Figure 10 shows the evolution of V_C/V_{NA} with TOS.[45,46]

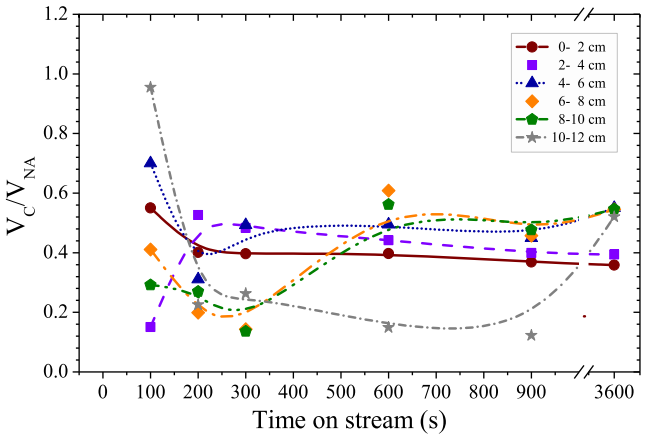

Figure 10. V_C/V_{NA} evolution with TOS.

V_C is the weight of carbonaceous deposits determined by TGA and divided by the estimated density of carbonaceous deposits (assumed to be 1 g·cm^{-3}), and V_{NA} is determined by CO_2 adsorption as the volume of the fresh catalyst minus that of the used catalyst. A low value of V_C/V_{NA} would imply that a small amount of coke blocks a large pore volume, which would agree with a pore mouth blockage mechanism and would suggest the existence of an internal mass transfer limitation.

The evolution of V_C/V_{NA} showed a different deactivation route as a function of the height in the catalytic bed. In the first section of the reactor, values of V_C/V_{NA} of around 0.6 could indicate that the deactivation started with the inner blockage of the active sites due to methanol transformation. This value diminished with the TOS, which could indicate the evolution of confined species and the partial blockage of pores. For lower sections, the deactivation started with the blockage of access points to pores, maybe due to the reaction of large products from the sections above, with less diffusivity, as is shown by the lower V_C/V_{NA} values. With the TOS, this blockage was substituted by the growth of molecules from methanol/1,2-dimethoxyethane inside the cages of the catalyst, which made V_C/V_{NA} values increase to those obtained in the upper sections of the catalyst bed.

The acidity of the catalyst is one of the most relevant parameters to analyze since it is the one that provides the activity to transform methanol into olefins.[47] Due to this evidence, a change in the acidity of the catalyst modifies its capability to transform methanol into dimethyl ether and later into olefins, paraffins, or cyclic molecules. Furthermore, it has been observed that when the catalyst loses the activity to transform methanol into hydrocarbons, it is still capable of producing methane and carbon monoxide from it.[17] The acid sites of the catalyst can be classified as a function of the temperature in which they are found in the desorption step of the TPD analysis. They could be classified as weak for 100−300 °C or as strong for 300−500 °C.

Figure 11 shows the evolution of weak acid site concentration as a function of the TOS for all catalyst bed heights.

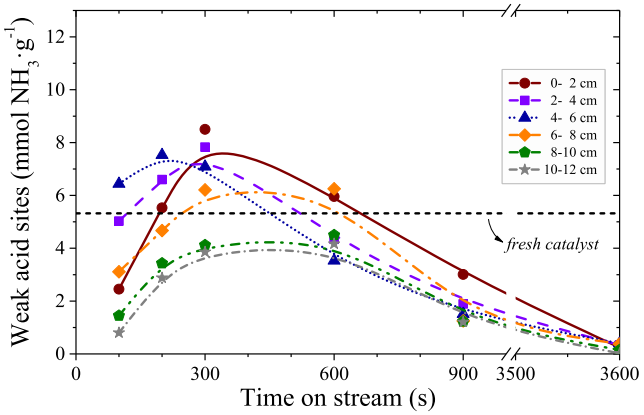

Figure 11. Weak acid site concentration evolution with the TOS.

The evolution of weak acid sites showed a clear trend with the TOS, which is also similar for all bed heights. During the first 100 s, the reaction took place in the 0−2 cm section, and a group of low-weight hydrocarbon species were formed. These were mainly methoxyl groups (Si−OH− CH_2, Al−OH−CH_2, and P−OH−CH_2) in the upper sections and products (light olefins) in the lower sections. As some of these were adsorbed on the acid sites, the weak acidity of the catalyst is lower than the original.[42,44]

Over the next few minutes, the weak acidity in all sections of the catalyst increased up to a maximum at 300 s. This could be caused by the reaction profile, which has reached the 6−8 cm section at that time. For the sections above, the catalyst acid sites were occupied by a mixture of methoxyl groups and other hydrocarbons with high weak acidity, which made the catalyst more acidic than the fresh one.[42,48] After that time, the total weak acidity decreased due to the formation of higher-weight species, which are less acidic. At 3600 s, all sites were blocked

https://doi.org/10.1021/acs.iecr.1c02718
Ind. Eng. Chem. Res. 2021, 60, 16162−16170

with these lower-acidity species, and thus, the weak acid site concentration was approximated to zero.

Figure 12 shows the evolution of the strong acid site concentration as a function of the TOS for all catalyst bed heights.

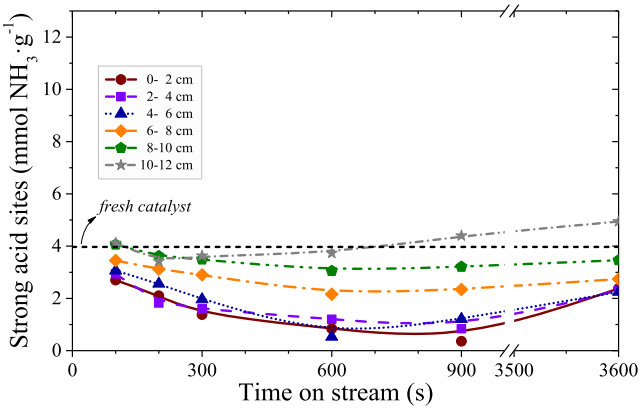

Figure 12. Strong acid site concentration evolution with the TOS.

The evolution of strong acid sites showed a trend with the TOS that differs from that observed in weak acid sites. In this case, the acidity of the catalyst at 100 s is lower than that of the fresh catalyst for all sections of the bed.

After the initial minutes of the reaction, in which the reaction occurs in the upper sections of the bed, the strong acid site concentration decreased to a minimum between 600 and 900 s. This could be caused by the formation of less acidic species, which did nothing but occupy these centers, causing the acidity to decrease. On the other hand, the lower sections of the bed did not show this decrease in the strong acidity but retained that of the fresh catalyst until the appearance of the reaction profile between 600 and 900 s, when it began to increase.

At longer times, the species adsorbed on the strong acid sites could have evolved toward more reactive and more acidic species or simply be desorbed, leaving the strong centers free, which increases the concentration of these acid sites.

In addition to the acid site concentration, TPD analysis allows the calculation of the relation between physisorbed and chemisorbed ammonia. Due to its small kinetic diameter (2.6 Å[20]), ammonia can diffuse along the micropores of the zeolite even when they are partially blocked by hydrocarbon molecules. The chemisorption contribution is shown in Figure 13.

The contribution of the chemisorption of ammonia shows a clear trend with the TOS. As can be seen, at 100 s, the reaction profile reached the 0−2 cm section, and products have been produced. These products of the reaction could have been adsorbed by the sections below and occupied some of the acid sites of the catalyst, decreasing the chemisorption. In the next minutes, the chemisorption contribution decreases as more products are formed and adsorbed in the acid sites. At longer times, the catalyst was deactivated, but some strong acidity remained, giving all sections of the catalyst bed around 20% chemisorption capacity.

Because of how weak and strong acidities evolve with the TOS, it is possible to conclude that the transformation of methanol into olefins would take place on the weak acid sites since they are the ones that present activity in the first minutes

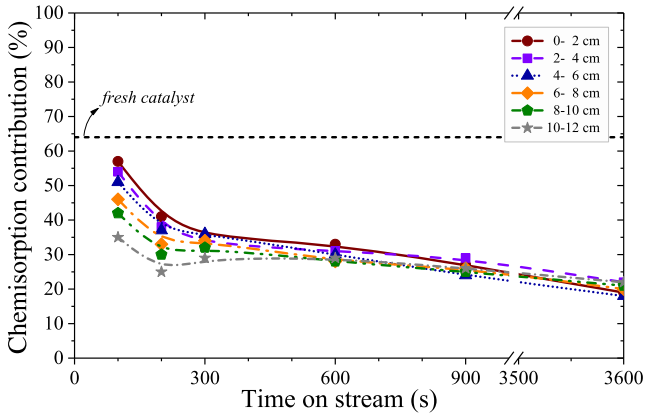

Figure 13. Chemisorption contribution evolution with the TOS.

of reaction, in which olefins are obtained as main products. On the other hand, the secondary mechanism mentioned above would occur in strong acid sites at long reaction times since they are the only ones that present activity when the products obtained are CH_4 and CO.

CONCLUSIONS

The deactivation of a SAPO-34 zeolite-based catalyst during the "MTO" process in a fixed-bed reactor has been studied. To achieve this, the feeding of methanol (diluted with nitrogen) in pulses was used. After each one of them, the catalyst bed was extracted by 2 cm sections.

The catalyst has been prepared by the agglomeration of zeolite SAPO-34, a clay, and an oxide. In order to verify the capability to agglomerate the zeolite, agglomeration tests have been carried out with various clays (five in all) and two oxides. The catalysts selected has been SAPO-34/bentonite/alumina in a 50/30/20 weight ratio as it is the one with the largest particle size between 160 and 315 μm (wt 75%).

The initial characterization of the catalyst shows that the agglomeration does not affect the microporous properties of the zeolite, which are fundamental for the MTO process since the porous structure of the final catalyst is a weighted average of its components in the selected proportion. The same effect has been found with acidity, which is responsible for the transformation of methanol into hydrocarbons. Finally, the analysis by FESEM and XRF corroborates the above with regard to agglomeration since the elemental composition of the catalyst is weighted with its components.

Regarding the deactivation of the catalyst and its evolution with the addition of methanol, it is possible to observe the deactivation profile macroscopically and obtain the rate at which it advances through the bed. This rate is not linear but increases for short times (100−300 s) as a result of the rapid formation of active species in the catalyst structure. After 300 s of methanol addition, the rate of the deactivation profile decreases drastically, an effect that can be attributed to a secondary mechanism of transformation of methanol into CH_4 and CO. This result has been found in a previous work[8] and is attributed to the retained acidity of the deactivated catalyst. This means that the same amount of methanol was not fed to the lower sections of the catalyst as that to the upper ones, so the deactivation rate is reduced.

The deactivation of the catalyst results in a change in its properties, either its micropore volume, the species retained in its structure, or its acidity.

https://doi.org/10.1021/acs.iecr.1c02718
Ind. Eng. Chem. Res. 2021, 60, 16162−16170

The micropore volume of CO_2 of the catalyst is modified as the deactivation takes place. This volume decreased rapidly in the upper sections and slowly in the lower sections, being more pronounced at short addition times of methanol. The decrease in the micropore volume could be attributed to the formation and accumulation of species in the catalyst structure. Because of this circumstance, CO_2 was not allowed to adsorb in it. In addition to this, when the steady state is reached (3600 s of methanol addition), the catalyst had a homogeneous appearance, although the upper sections have less micropore volume than the lower ones.

The evolution in the micropore volume could be attributed to the presence of species retained in the structure of the catalyst. These include a wide range of species of different natures that have been classified by TGA as volatile or nonvolatile species, according to the temperature at which they are released and whether they require oxygen for it. The results show that volatile species were formed rapidly in the first methanol pulses and stabilized at a constant concentration. On the other hand, nonvolatile species were formed more gradually, but they accumulate progressively in the catalyst structure, deactivating it.

The evolution of the deactivation profile could be caused by an evolution in the acidity of the catalyst, which presents a different trend depending on whether the acid sites are weak or strong. For weak acid sites, there was an initial increase in their concentration, caused by the rapid formation of species with higher acidity, causing the reaction rate to increase. The weak acidity of the catalyst showed a maximum value around 300 s of methanol addition, then decreased down to zero. For strong acid sites, the trend was the opposite. Initially, the acidity decreased to a minimum (between 600 and 900 s), but later, it increased up to a value different from zero. This strong residual acidity could be the reason for the previously mentioned secondary mechanism.

AUTHOR INFORMATION

Corresponding Author

Miguel Menéndez − *Aragón Institute for Engineering Research (I3A), University of Zaragoza, 50018 Zaragoza, Spain;* orcid.org/0000-0002-2494-102X; Email: qtmiguel@unizar.es

Authors

Diego Zapater − *Aragón Institute for Engineering Research (I3A), University of Zaragoza, 50018 Zaragoza, Spain*

Javier Lasobras − *Aragón Institute for Engineering Research (I3A), University of Zaragoza, 50018 Zaragoza, Spain*

Jaime Soler − *Aragón Institute for Engineering Research (I3A), University of Zaragoza, 50018 Zaragoza, Spain*

Javier Herguido − *Aragón Institute for Engineering Research (I3A), University of Zaragoza, 50018 Zaragoza, Spain*

Complete contact information is available at: https://pubs.acs.org/10.1021/acs.iecr.1c02718

Notes

The authors declare no competing financial interest.

ACKNOWLEDGMENTS

Financial support from MINECO Project CTQ2016-76533-R is gratefully acknowledged.

REFERENCES

(1) Chang, C.; Silvestri, A. J. The conversion of methanol and other O-compounds to hydrocarbons over zeolite catalysts. *J. Catal.* **1977**, *47*, 249.

(2) Chang, C.; Chu, C. T. W.; Socha, R. F. Methanol conversion to olefins over ZSM-5 I. Effect of temperature and zeolite SiO_2/Al_2O_3. *J. Catal.* **1984**, *86*, 289.

(3) Chu, C.; Chang, C. D. Methanol conversion to olefins over ZSM-5 II. Olefin distribution. *J. Catal.* **1984**, *86*, 297.

(4) Baerlocher, C.; McCusker, L. B. Database of Zeolite Structures, http://www.iza-structure.org/databases/ (accessed October 15, 2021).

(5) Catlow, C. R. A.; Bell, R. G.; Gale, J. D.; Lewis, D. W. Modelling of structure and reactivity in zeolites. *Stud. Surf. Sci. Catal.* **1995**, *97*, 87.

(6) Dessau, R.; LaPierre, R. B. On the mechanism of methanol conversion to hydrocarbons over HZSM-5. *J. Catal.* **1982**, *78*, 136.

(7) Dessau, R. On the H-ZSM-5 catalyzed formation of ethylene from methanol or higher olefins. *J. Catal.* **1986**, *99*, 111.

(8) Dahl, I. M.; Kolboe, S. On the reaction mechanism for propene formation in the MTO reaction over SAPO-34. *Catal. Lett.* **1993**, *20*, 329.

(9) Haw, J. F.; Song, W.; Marcus, D. M.; Nicholas, J. B. The mechanism of methanol to hydrocarbon catalysis. *Acc. Chem. Res.* **2003**, *36*, 317.

(10) Arstad, B.; Kolboe, S. Methanol-to-hydrocarbons reaction over SAPO-34. Molecules confined in the catalyst cavities at short time on stream. *Catal. Lett.* **2001**, *71*, 209.

(11) Wang, W.; Hunger, M. Reactivity of surface alkoxy species on acidic zeolite catalysts. *Acc. Chem. Res.* **2008**, *41*, 895.

(12) Bjorgen, M.; Svelle, S.; Joensen, F.; Nerlov, J.; Kolboe, S.; Bonino, F.; Palumbo, L.; Bordiga, S.; Olsbye, U. Conversion of methanol to hydrocarbons over zeolite H-ZSM-5: On the origin of the olefinic species. *J. Catal.* **2007**, *249*, 195.

(13) Svelle, S.; Aravinthan, S.; Bjorgen, M.; Lillerud, K.; Kolboe, S.; Dahl, I.; Olsbye, U. The methyl halide to hydrocarbon reaction over H-SAPO-34. *J. Catal.* **2006**, *241*, 243.

(14) Bjørgen, M.; Lillerud, K. P.; Olsbye, U.; Svelle, S. Conversion of methanol to hydrocarbons: Hints to rational catalyst design from fundamental mechanistic studies on H-ZSM-5. *Stud. Surf. Sci. Catal.* **2007**, *167*, 463−468.

(15) Fu, H.; Song, W.; Haw, J. F. Polycyclic aromatics formation in HSAPO-34 during methanol-to-olefin catalysis: Ex situ characterization after cryogenic grinding. *Catal. Lett.* **2001**, *76*, 89.

(16) Wragg, D. S.; O'Brien, M. G.; Bleken, F. L.; Di Michiel, M.; Olsbye, U.; Fjellvåg, H. Watching the methanol-to-olefin process with time- and space-resolved high-energy operando X-ray diffraction. *Angew. Chem., Int. Ed.* **2012**, *51*, 7956.

(17) Zapater, D.; Lasobras, J.; Soler, J.; Herguido, J.; Menéndez, M. Counteracting SAPO-34 catalyst deactivation in MTO process using a two zone fluidized bed reactor: Reactor testing and process viability. *Catal. Today* **2021**, *362*, 155−161.

(18) Ismail, A. F.; Khulbe, K. C.; Matsuura, T. *Gas Separation Membranes: Polymeric and Inorganic*; Springer, 2015.

(19) Shang, H.; Li, Y.; Liu, J.; Tang, X.; Yang, J.; Li, J. CH_4/N_2 separation on methane molecules grade diameter channel molecular sieves with a CHA-type structure. *Chin. J. Chem. Eng.* **2019**, *27*, 1044.

(20) Breck, D. W. *Zeolite Molecular Sieves. Structure, Chemistry and Use*; John Wiley and Sons, 1974.

(21) Bräuer, P.; Ng, P. L.; Situmorang, O.; Hitchcock, I.; D'Agostino, C. Effect of Al content on number and location of hydroxyl acid species in zeolites: A DRIFTS quantitative protocol without the need for molar extinction coefficients. *RSC Adv.* **2017**, *7*, 52604.

(22) Park, J. W.; Lee, J. Y.; Kim, K. S.; Hong, S. B.; Seo, G. Effects of cage shape and size of 8-membered ring molecular sieves on their deactivation in methanol-to-olefin (MTO) reactions. *Appl. Catal., A* **2008**, *339*, 36.

(23) Aguayo, A. T.; Campo, A. E. S. d.; Gayubo, A. G.; Tarrío, A.; Bilbao, J. Deactivation by coke of a catalyst based on a SAPO-34 in the transformation of methanol into olefins. *J. Chem. Technol. Biotechnol.* **1999**, *74*, 315.
(24) Ilias, S.; Bhan, A. Mechanism of the catalytic conversion of methanol to hydrocarbons. *ACS Catal.* **2013**, *3*, 18.
(25) Dai, W.; Wu, G.; Li, L.; Guan, N.; Hunger, M. Mechanisms of the deactivation of SAPO-34 materials with different crystal sizes applied as MTO catalysts. *ACS Catal.* **2013**, *3*, 588.
(26) Epelde, E.; Ibañez, M.; Aguayo, A. T.; Gayubo, A. G.; Bilbao, J.; Castaño, P. Differences among the deactivation pathway of HZSM-5 zeolite and SAPO-34 in the transformation of ethylene or 1-butene to propylene. *Microporous Mesoporous Mater.* **2014**, *195*, 284.
(27) Charghand, M.; Haghighi, M.; Saedy, S.; Aghamohammadi, S. Efficient hydrothermal synthesis of nanostructured SAPO-34 using ultrasound energy: Physicochemical characterization and catalytic performance toward methanol conversion to light olefins. *Adv. Powder Technol.* **2014**, *25*, 1728.
(28) Hereijgers, B. P. C.; Bleken, F.; Nilsen, M. H.; Svelle, S.; Lillerud, K.-P.; Bjørgen, M.; Weckhuysen, B. M.; Olsbye, U. Product shape selectivity dominates the Methanol-to-Olefins (MTO) reaction over H-SAPO-34 catalysts. *J. Catal.* **2009**, *264*, 77.
(29) Hajiashrafi, T.; Nemati Kharat, A. Study of preparation methods and their effect on the morphology and texture of SAPO-34 for the methanol to olefin reaction. *React. Kinet., Mech. Catal.* **2013**, *108*, 417.
(30) Gayubo, A. G.; Aguayo, A. T.; Benito, P. L.; Landeta, A.; Castilla, M.; Bilbao, J. Reactivation of the HZSM-5 Zeolite-Based Catalyst Used in the MTG Process. *AIChE J.* **1997**, *43*, 1551.
(31) Sánchez del Campo, A. E.; Gayubo, A. G.; Aguayo, A. T.; Tarrío, A.; Bilbao, J. Acidity, surface species, and mechanism of methanol transformation into olefins on a SAPO-34. *Ind. Eng. Chem. Res.* **1998**, *37*, 2336−2340.
(32) Konnov, S. V.; Pavlov, V. S.; Kots, P. A.; Zaytsev, V. B.; Ivanova, I. I. Mechanism of SAPO-34 catalyst deactivation in the course of MTO conversion in a slurry reactor. *Catal. Sci. Technol.* **2018**, *8*, 1564−1577.
(33) Gopalakrishnan, S.; Viswanathan, K. R.; Vishnu Priya, S.; Herbert Mabel, J.; Palanichamy, M.; Murugesan, V. Synthesis of 7-hydroxy-4-methyl coumarin over Lewis acid metal ion-exchanged ZAPO-5 molecular sieves. *Microporous Mesoporous Mater.* **2009**, *118*, 523.
(34) Freitas, C.; Barrow, N. S.; Zholobenko, V. Accessibility and Location of Acid Sites in Zeolites as Probed by Fourier Transform Infrared Spectroscopy and Magic Angle Spinning Nuclear Magnetic Resonance. *Johnson Matthey Technol. Rev.* **2018**, *62*, 279.
(35) Kang, M. Methanol conversion on metal-incorporated SAPO-34s (MeAPSO-34s). *J. Mol. Catal. A: Chem.* **2000**, *160*, 437−444.
(36) Kang, M.; Inui, T. Effects of decrease in number of acid sites located on the external surface of Ni-SAPO-34 crystalline catalyst by the mechanochemical method. *Catal. Lett.* **1998**, *53*, 171.
(37) van Niekerk, M. J.; Fletcher, J. C. Q.; O'Connor, C. T. Effect of catalyst modification on the conversion of methanol to light olefins over SAPO-34. *Appl. Catal., A* **1996**, *138*, 135.
(38) Townsend, R. P.; Coker, E. N. Chapter 11 Ion exchange in zeolites. *Stud. Surf. Sci. Catal.* **2001**, *137*, 467.
(39) Calabria, J. A. A.; Amaral, D. N.; Ladeira, A. C. Q.; Cota, S. D. S.; Silva, T. S. S. Determination of the cation exchange capacity of bentonite exposed to hyperalkaline fluid. *Int. Nucl. Atl. Conf.* **2013**, *45*, 27.
(40) Dorado, F.; Romero, R.; Cañizares, P. Influence of clay binders on the performance of Pd/HZSM-5 catalysts for the hydroisomerization of n-butane. *Ind. Eng. Chem. Res.* **2001**, *40*, 3428.
(41) Li, Y. Y.; Perera, S. P.; Crittenden, B. D.; Bridgwater, J. The effect of the binder on the manufacture of a 5A zeolite monolith. *Powder Technol.* **2001**, *116*, 85.
(42) Haw, J. F.; Marcus, D. M. Well-defined (supra)molecular structures in zeolite methanol-to-olefin catalysis. *Top. Catal.* **2005**, *34*, 41.
(43) Obrzut, D. L.; Adekkanattu, P. M.; Thundimadathil, J.; Liu, J.; Dubois, D. R.; Guin, J. A. Reducing methane formation in methanol to olefins reaction on metal impregnated SAPO-34 molecular sieve. *React. Kinet. Catal. Lett.* **2003**, *80*, 113.
(44) Luo, M.; Zang, H.; Hu, B.; Wang, B.; Mao, G. Evolution of confined species and their effects on catalyst deactivation and olefin selectivity in SAPO-34 catalyzed MTO process. *RSC Adv.* **2016**, *6*, 17651.
(45) Zhang, X.; Wang, Y.; Xin, F. Coke deposition and characterization on titanium silicalite-1 catalyst in cyclohexanone ammoximation. *Appl. Catal., A* **2006**, *307*, 222.
(46) Feng, X.; Duan, X.; Qian, G.; Zhou, X.; Chen, D.; Yuan, W. Au nanoparticles deposited on the external surfaces of TS-1: Enhanced stability and activity for direct propylene epoxidation with H_2 and O_2. *Appl. Catal., B* **2014**, *150-151*, 396.
(47) Nesterenko, N.; Aguilhon, J.; Bodart, P.; Minoux, D.; Dath, J.-P. Methanol to Olefins: An Insight Into Reaction Pathways and Products Formation. In *Zeolites Zeolite-like Materials*; Elsevier, 2016; Chapter 5, p 189.
(48) Maache, M.; Janin, A.; Lavalley, J. C.; Benazzi, E. FT infrared study of Brønsted acidity of H-mordenites: Heterogeneity and effect of dealumination. *Zeolites* **1995**, *15*, 507.

https://doi.org/10.1021/acs.iecr.1c02718
Ind. Eng. Chem. Res. 2021, 60, 16162−16170